Turkish Journal of Electrical Engineering & Computer Sciences
http://journals.tubitak.gov.tr/elektrik/
Research Article

Turk J Elec Eng & Comp Sci
(2015) 23: 335 – 353
© TÜBİTAK
doi:10.3906/elk-1212-11

A particle swarm optimization-based approach to achieve optimal design and operation strategy of standalone hybrid energy systems

Mahram GHAZVINI, Ali ABBASPOUR-TEHRANI-FARD, Mahmud FOTUHI-FIRUZABAD*
Center of Excellence in Power System Control and Management, Department of Electrical Engineering,
Sharif University of Technology, Tehran, Iran

Received: 02.12.2012 • **Accepted:** 15.02.2013 • **Published Online:** 23.02.2015 • **Printed:** 20.03.2015

Abstract: As a cost-effective and reliable alternative to supply remote areas, standalone hybrid energy systems (HESs) are recently under investigation to address various concerns associated with technical, financial, and environmental issues. This paper presents a comprehensive algorithm that can simultaneously optimize the component size, operation strategy, and slope of the photovoltaic panels of a standalone HES using an improved variant of particle swarm optimization (PSO), designated as the passive congregation PSO. A new operation strategy is proposed based on the set points of the control system. The optimization algorithm determines the optimal values of the set points to efficiently optimize the HES operation. The applicability and effectiveness of the proposed method are investigated through some numerical analyses performed on a practical remote area in Iran. In doing so, the proposed method is applied to various HES configurations and the results are compared with those obtained using the existing methods. Several load growth and wind speed scenarios are considered, and their impacts on the optimization results are examined.

Key words: Hybrid energy system, optimal operation strategy, passive congregation particle swarm optimization, unit-sizing

1. Introduction

Due to dispersed population and rugged terrain, utility grid extension is uneconomical for many remote areas in developing countries. High fuel prices, emissions, costly fuel transportation, growing interest in green development, and the cost reduction trend of renewable technologies are the motivations for integrating renewable resources with fossil fuel technologies. Hybrid energy systems (HESs), composed of renewable resources, fossil fuel generators, and storage devices, have advantages of both renewable and fossil fuel technologies. HESs not only decrease the fuel consumption and maintenance costs of diesel generators, but also reduce the effects of the unpredictable and costly nature of renewable energies.

Standalone HESs should compete with other alternatives such as grid extension and diesel-only systems. Both reliability and economic issues play important roles in the competition. Therefore, an optimization technique is essential to minimize the cost while maintaining reliability. Considerable research has been conducted on the optimal unit-sizing aspect of the problem without considering an optimal operation strategy [1]. The authors in [2] presented optimal unit-sizing of a wind-battery HES in Turkey. An optimization procedure based on the genetic algorithm was presented in [3] to optimize the component size of a grid-connected HES. In [4], the component size of a grid-connected HES was optimized in order to minimize the cost and emissions and

*Correspondence: fotuhi@sharif.edu

maximize the reliability using a modified particle swarm optimization (PSO) algorithm. A PSO-based method was proposed in [5,6] for optimal sizing of the HES. In [7], an optimal unit-sizing algorithm for a HES using the conventional PSO was presented. The abovementioned papers did not consider an operation optimization scheme in their proposed methods.

One of the earliest works in optimizing the HES operation strategy was reported in [8]. In [9], starting and stopping set points of diesel generators were used to optimize the control strategy. The authors in [10] presented an optimal control strategy based on minimizing diesel generator participation and maximizing the renewable energy fraction. In [11], a real-time PSO-based optimal operation strategy for a HES without considering a unit-sizing scheme was presented. The authors in [12,13] used the genetic algorithm to optimize the component size and control strategy of the HES. However, the impact of the load growth in the design and operation of the HES was neglected in their studies.

Most of the reported works have focused on optimizing either the component size or operation strategy, but have not optimized both. In other words, these procedures have neglected important aspects of the optimization problem. This drawback may create important errors, as the net present cost (NPC) of the HES depends on both the component size and the operation strategy. Hence, considering an optimal unit-sizing scheme without optimizing the operation strategy may cause the algorithm to be trapped in local minima. In addition, the impact of the load growth on the HES design and operation was not considered in the previous studies, while it is investigated in the current paper. Load growth should be investigated in the optimization of the HES to assure acceptable reliability in practical applications, where the electrical demand increases over time. Another contribution of the current study is that in contrast to previous studies that have focused on serving the electrical load, this paper presents a scheme to simultaneously supply the electrical, thermal, and water demands of remote areas.

This paper aims to simultaneously optimize the component size, operation strategy, and photovoltaic (PV) slope of standalone HESs using the passive congregation PSO (PSOPC). The objective is to achieve the optimal design and operation of a HES at minimum cost in serving the electrical and thermal loads, as well as the water demand, of remote areas subject to physical and reliability constraints. In this regard, the excess energy of the renewable resources is utilized to pump water and store it in a tank for domestic uses. Moreover, the waste heat of the diesel generator and dump load is recovered and used to serve the thermal loads. Hence, the energy resources are more efficiently employed compared to studies presented in previous papers [12–14]. To effectively optimize the operation strategy of the HES, the proposed optimization algorithm determines the optimal set points of the control system. In this regard, new control set points are defined for the HES, and a new operation strategy is presented based on the defined set points. In order to show the effectiveness of the defined set points, the proposed PSOPC approach is compared with a PSOPC unit-sizing method. The latter is similar to the proposed PSOPC, but does not optimize the control set points.

2. Hybrid energy system modeling procedure

In this section, the modeling procedure of the components of the HES, as well as the proposed operation strategy, are briefly described. Figure 1 shows the schematic of the HES investigated in this paper. The excess energy of the renewable resources is utilized to supply the deferrable load (a water pump) and the dump load (a bank of resistors) considering their priority. Figure 1 also depicts the electrical and thermal energy flows among the components.

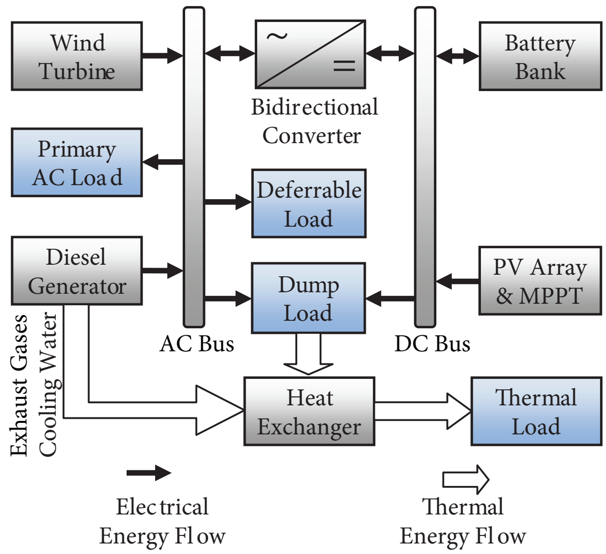

Figure 1. General schematic of the HES.

2.1. PV array

The incident radiation on the tilted PV surface can be estimated considering the solar radiation and ambient temperature data, latitude and longitude of the site, and slope of the PV panels [15,16]. At each time step t, considering the incident radiation on the tilted PV surface and the cell efficiency, the output power of the PV array P_{pv}^t is calculated as expressed in Eq. (1).

$$P_{pv}^t = A_{pv}.\eta_{mppt}.\eta_{mp}^t.G_T^t \tag{1}$$

$$A_{pv} = P_{pv,r}/\eta_{mp,STC} \tag{2}$$

The PV array is equipped with a maximum power point tracker (MPPT) to extract maximum power from the PV cells. Therefore, the DC bus voltage can be neglected in the PV model.

2.2. Wind turbine

The output power of the wind turbine is a nonlinear function of the wind speed given by the power curve. Figure 2 depicts the normalized power curve of the Atlantic Orient AOC 15/50 wind turbine utilized in the current study [17]. The impacts of the turbine's hub height, roughness of the terrain, and air density (as a function of the altitude) on the output power are also considered [18].

2.3. Diesel generator

At time step t, the output power of the diesel generator is obtained using Eq. (3):

$$P_g^t = U_g^t.\min\left(P_{g,r}, Max(P_{g,\min}, P_L^t + P_p^t + P_{dump}^t - P_w^t - P_c^t)\right), \tag{3}$$

where P_c^t is the converter's output power, which is positive in the inverter mode and negative in the rectifier mode. The fuel consumption characteristic of a diesel generator is approximately a linear function of its output power, which is shown in Eq. (4) [19].

$$F_g^N = \sum\nolimits_{t=1}^{8760} (F_0 \,.\, P_{g,r} + F_1 \,.\, P_g^t) \,.\, U_g^t \tag{4}$$

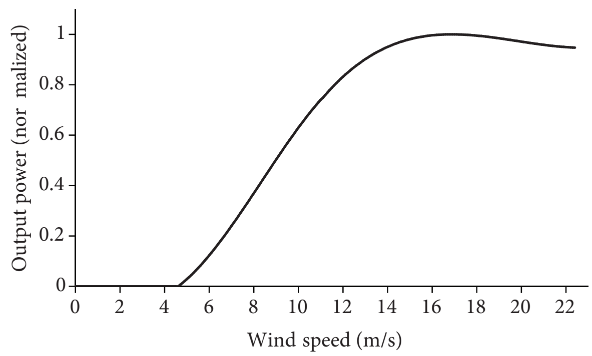

Figure 2. Normalized power curve of the AOC 15/50 wind turbine [17].

2.4. Battery bank

The kinetic battery model is used in this study [18,20,21]. It is known that the battery capacity decreases with increasing charge/discharge rates. For modeling this characteristic, the total energy of the battery is assumed to comprise the available and bound energies [20]. The available energy Q_1^t is the energy that is immediately available for use, while the bound energy Q_2^t can be released at a constant rate. The battery state of charge (SOC) can be written as in Eq. (5) [20]:

$$soc^t = 100 \;\times\; (Q_1^t + Q_2^t)/P_{b,r}. \tag{5}$$

The ampere-hour throughput method is used to estimate the battery lifetime [22]. It assumes that a fixed amount of energy, designated as the lifetime throughput, can be cycled through a battery before its replacement. In addition, the battery model considers the battery float life in the lifetime estimation.

2.5. Power converter

It is assumed that the converter has a constant no-load loss and a loss proportional to the converted power [21]. Eq. (6) gives the converter efficiency η_c^t as a function of its output power:

$$\eta_c^t = \frac{|P_c^t|}{P_{c,in}^t} = \left(\frac{1}{\eta_{c,r}} + \frac{P_{c,NL}}{|P_c^t|} - \frac{P_{c,NL}}{P_{c,r}}\right)^{-1}. \tag{6}$$

It can be seen from Eq. (6) that the converter efficiency gets worse at lower output powers.

2.6. Deferrable load

Deferrable loads are defined as the electrical loads that must be met within a specific period, but the exact timing is not important. In this study, a water pumping system is incorporated into the HES, as a deferrable load, to supply the water demands of a remote area using the surplus energy produced by renewable resources. Eq. (7) gives the water content of the tank at the end of day d:

$$W_{tank}^d = Min(C_{tank}\,,\, Max(0,\, W_{tank}^{d-1} + \sum_{t=1}^{24} (\frac{P_p^t \,.\, F_{p,max}}{P_{p,r}}) - D_w^d)), \quad P_{p,min} \le P_p^t \le P_{p,r}. \tag{7}$$

2.7. Heat recovery

Thermal loads can be supplied using the recovered thermal energy from the exhaust gases and cooling water of the diesel generator. In generators with reciprocating engines, approximately 49% of the input energy of the fuel can be recovered in the form of thermal energy [23]. In addition, the dump load absorbs the surplus energy produced by renewable resources and converts it to useful thermal energy. The efficiency of the conversion is assumed to be 90%. In this study, the deferrable load has higher priority to absorb the surplus energy than the dump load.

2.8. The proposed operation strategy

Here the proposed operation strategy of the HES is described. The entire operation period of the HES is divided into equal time steps, and the operation strategy is consecutively run for all of the time steps. In this regard, renewable resources are first utilized to serve the electrical load as much as possible. Next, the remaining load, namely the net load, is met by employing the battery or diesel generator. The cost per kilowatt-hour of the energies supplied by the battery and diesel generator is used as a criterion to choose the most cost-effective option, the battery or diesel generator. Two dispatch strategies, load following and cycle charging, are considered for the diesel generator [10]. The load following strategy indicates that the diesel generator produces enough power to serve the net load, but it does not charge the battery. However, in the cycle charging, the generator not only serves the net load, but also charges the battery as much as possible.

The following control set points are defined and integrated into the proposed operation strategy. The optimization algorithm searches for the optimal values of the set points to achieve an optimal operation scheme.

- Diesel running threshold, $P_{trs,g}$: Once the diesel generator is off and the renewable and battery powers are unable to meet the load, it may be more economical to keep the generator off and accept some unmet energy as long as the unmet load is less than $P_{trs,g}$.

- Battery discharge limit, $P_{lim,b}$: This set point limits the battery discharge power to an appropriate value to avoid battery power shortage in the future.

- Battery maximum SOC, $soc_{\max}$: The maximum power that can be absorbed by the battery decreases as the SOC increases. The charge controller prevents the diesel generator from charging the battery when $soc^t \geq soc_{\max}$ due to poor efficiency of the converter at low powers.

- SOC threshold, soc_{trs}: This set point prevents the battery from supplying the load when the generator is off and $soc^t < soc_{trs}$. In this case, the generator should be started even if the battery is more economical than the generator. However, in the case of a power shortage, both of the battery and generator are discharged, even if $soc^t < soc_{trs}$.

- SOC set point, soc_{sp}: This set point has been defined as a criterion to choose the cycle charging or load following strategies. If $soc^t > soc_{sp}$, the load following is selected; otherwise, the cycle charging will be employed.

The step-by-step algorithm of the proposed operation strategy can be summarized as follows:

Step 1: Read the input data, including the technoeconomic data of the components and historical data of the wind speed, solar radiation, ambient temperature, and electrical load.

Step 2: At each time step, compare the output powers of the PV array and wind turbine with the electrical load. If the renewable power exceeds the electrical load, charge the battery as much as possible, use the remaining energy (if any) to serve the deferrable and dump loads considering their priority, and then go to step 8; otherwise, calculate the net load and go to the next step.

Step 3: If the following conditions are satisfied, utilize the battery power and go to step 8; otherwise, go to step 4:

1. The battery power and the converter capacity are sufficient to satisfy the net load,
2. Using the battery is more economical than the diesel generator,
3. The battery discharge power is less than $P_{lim,b}$,
4. The battery SOC is greater than soc_{trs}.

Step 4: If *net-load* $\geq P_{trs,g}$, start the diesel generator and go to step 5; otherwise, keep the generator off, calculate the unmet energy, and go to step 9.

Step 5: If the diesel generator meets the net load, go to the next step; otherwise, go to step 7.

Step 6: Employ the proper dispatch strategy, load following or cycle charging, based on the soc_{sp} set point. Charge the battery, and use the remaining energy (if any) to serve the deferrable and dump loads considering their priority. If the water level in the tank (Eq. (7)) drops below a critical value (here, 25%), make the diesel generator produce additional power to keep the water level above the critical value. Go to step 8.

Step 7: If the diesel generator is unable to meet the net load, run the generator at its rated power and utilize the battery to meet the net load. Finally, if the renewable resources, diesel generator, and battery cannot meet the load, calculate the amount of unmet energy.

Step 8: Calculate the new SOC of the battery using Eq. (5).

Step 9: Repeat steps 2 to 8 for all of the time steps.

Step 10: Estimate the NPC and loss of energy expectation (LOEE) of the HES (see Sections 3.1 and 3.2).

3. Problem statement

In this paper, the HES is optimized considering the NPC as the objective function. Running the operation strategy (Section 2.8) gives the NPC value.

The optimization procedure considers 2 aspects of the unit-sizing and operation strategy, which are both correlated. This indicates that an operation strategy, which is optimal for a certain system sizing, may not be optimal for other component sizes and vice versa. It is important to simultaneously optimize both aspects of the unit-sizing and operation strategy, because the NPC of the HES depends on both of them. As a result, considering an optimal unit-sizing scheme without optimizing the operation strategy (as performed in the previous studies) may cause the optimization algorithm to be trapped in local minima.

The optimization algorithm considers the following decision variables, as expressed in Eq. (8):

$$X = [P_{pv,r}, P_{w,r}, P_{g,r}, P_{c,r}, P_{b,r}, slope_{pv}, P_{trs,g}, P_{lim,b}, soc_{\max}, soc_{sp}, soc_{trs}]. \tag{8}$$

- Component size: Five decision variables (the first 5 elements of vector X) are dedicated to the sizes of the PV array, wind turbine, diesel generator, power converter, and battery bank to achieve an optimal unit-sizing scheme.

- Slope of the PV panels: The optimization algorithm determines the optimal value of the slope of the PV panels (the sixth element of vector X).
- Control set points: Five decision variables are dedicated to the control set points (the last 5 elements of vector X), which were described in Section 2.8. The optimization algorithm sets them to the appropriate values to attain an optimal operation strategy.

It deserves mentioning that the designer of the HES can utilize the proposed method to determine the optimal values of the component size and control set points. Once the HES starts operating, an online optimization method can be utilized to perform further modifications to the control set points to compensate for the impacts of various uncertainties on the HES operation. It should be noted that the online optimization of the control set points is not within the scope of the current paper and may be the subject of future works.

3.1. The cost objective function

The NPC of the HES is considered as the objective function to be minimized. Eq. (9) shows the various costs associated with the NPC.

$$NPC = C_I + C_{rep}^{PW} + C_{om}^{PW} + C_{fuel}^{PW} - S^{PW} \tag{9}$$

Here, C_I indicates the initial cost and C_{rep}^{PW} is the present worth of the components' replacement cost, which are expressed as the following equations:

$$C_I = \sum_{m=pv,w,g,b,c} (\alpha_{m,I}.\, P_{m,r}), \tag{10}$$

$$C_{rep}^{PW} = \sum_{m=pv,w,g,b,c} \left(\sum_{n=1}^{n_{m,rep}} \frac{\alpha_{m,rep}\,.\, P_{m,r}}{(1 + i)^{\left(\sum_{j=1}^{n} N_m^j\right)}} \right), \tag{11}$$

where $n_{m,rep}$ is the number of replacements of component m and N_m^j denotes the lifetime of component m, before its jth replacement.

The third term of Eq. (9), C_{om}^{PW}, denotes the operation and maintenance (O&M) cost of the components and can be expressed as in Eq. (12).

$$C_{om}^{PW} = \sum_{N=1}^{N_{pr}} \sum_{m=pv,w,b,c} \left(\frac{\alpha_{m,om}.\, P_{m,r}}{(1 + i)^N} \right) + \sum_{N=1}^{N_{pr}} \frac{\alpha_{g,om}.\, P_{g,r}.\, R_g^N}{(1 + i)^N} \tag{12}$$

The last 2 terms of Eq. (9) are, respectively, the present worth of the fuel cost and the salvage value, which can be obtained from Eq. (13).

$$C_{fuel}^{PW} = \sum_{N=1}^{N_{pr}} \frac{F_g^N\,.\, c_f}{(1 + i)^N} \quad , \quad S^{PW} = \sum_{m=pv,w,g,b,c} \frac{\alpha_{m,rep}.\, P_{m,r}.RL_m}{(1 + i)^{N_{pr}}} \tag{13}$$

It is assumed that the salvage value of component m is proportional to the percentage of its remaining lifetime RL_m at the end of the project lifetime.

3.2. Constraints

To satisfy the physical and practical limitations, each decision variable must satisfy the following inequality constraint:

$$x_d^{\min} \leq x_{id}^k \leq x_d^{\max}, \tag{14}$$

where $x_d^{\min}$ and $x_d^{\max}$ are the lower and upper limits of the dth decision variable in Eq. (8). The lower and upper limits on the decision variables are given in Table 1. Moreover, the following reliability constraint must be satisfied:

$$LOEE_{p.u.}^{ann} \leq LOEE_{p.u.}^{\max}, \tag{15}$$

where

$$LOEE_{p.u.}^{ann} = \frac{\sum_{t=1}^{8760} ENS^t}{\sum_{t=1}^{8760} E_d^t}. \tag{16}$$

Table 1. Lower and upper limits on the decision variables.

Decision variable	$P_{pv,r}$	$P_{w,r}$	$P_{g,r}$	$P_{c,r}$	$P_{b,r}$	$Slope_{pv}$	$P_{trs,g}$	$P_{lim,b}$	$soc_{\max}$	soc_{sp}	soc_{trs}
	kW	kW	kW	kW	kWh	°	kW	kW	%	%	%
Lower limit	0	0	0	0	0	15	0	0	80	80	30
Upper limit	300	300	300	300	3000	45	20	200	100	100	70

3.3. Implementation of the PSOPC algorithm

PSO has been successfully applied in many research and application areas. In [24] a comprehensive overview of PSO and its applications in a power system was provided and its advantages over the other optimization methods were discussed. The PSOPC approach is an improved version of the PSO, which uses extra information sharing among individuals to increase the population diversity and to enable the algorithm to escape from local minima [25]. Detailed information about the PSOPC algorithm and its advantages over the classic PSO were provided in [25,26].

The PSOPC approach maintains a population of the particles, where the position vector of each particle in the search space represents the vector of the decision variables (Eq. (8)). In other words, each particle represents a potential solution associated with the design and operation strategy of the HES. Particles move in the search space to explore better solutions. At iteration k of the PSOPC algorithm, each particle i updates its velocity and position vectors using the following equations [25,26]:

$$V_i^{k+1} = \omega^k .\, V_i^k + c_1 .\, r_1^k .(Pbest_i^k - X_i^k) + c_2 .\, r_2^k .(Gbest^k - X_i^k) + c_3 . r_3^k .(Rbest^k - X_i^k), \tag{17}$$

$$X_i^{k+1} = X_i^k + \chi \,.\, V_i^{k+1}. \tag{18}$$

A fitness value is assigned to each particle based on the NPC associated with the position vector of that particle. In addition, after moving each particle to a new position, it must satisfy the variables and LOEE constraints; otherwise, the particle returns to its primary position. It should be noted that, at each iteration of the PSOPC algorithm and for each particle, the proposed operation strategy is run to obtain the NPC and LOEE associated with that particle.

4. Study results

The proposed simulation and optimization algorithms are coded in the MATLAB environment. A 1-h time step is used to run the proposed operation strategy. The maximum iteration number of the algorithm is set to 300. Four HES configurations are considered as potential alternatives to supply the study area, a rural district in the eastern part of Iran (32° 47′N, 58° 47′E; altitude: 1000 m). Table 2 represents the components associated with each configuration. Table 3 summarizes the technoeconomic parameters of the HES [18].

Table 2. Potential configurations of the HES.

Configuration	PV array	Wind turbine	Diesel generator	Power converter	Battery bank
1	√	√	√	√	√
2			√		
3	√			√	√
4	√		√	√	√

Table 3. Technoeconomic parameters of the HES [18].

	Description	Value	Unit
PV	Lifetime	25	Years
	Initial/replacement costs	4700/4500	\$/kW
	O&M cost	0.1	\$/kW/year
	Efficiency under standard test conditions	15	%
	MPPT's efficiency	95	%
Wind turbine	Lifetime	20	Years
	Initial/replacement costs	3000/2700	\$/kW
	O&M cost	50	\$/kW/year
	Hub height	40	m
Diesel generator	Useful lifetime	20,000	h
	Initial/replacement costs	600/500	\$/kW
	O&M cost	0.05	\$/kW/h
	Minimum load ratio	30	%
	No-load fuel consumption	0.08	L/h/kW$_{rated}$
	Incremental fuel consumption	0.25	L/kWh$_{out}$
	Fuel price	0.4	\$/L
Battery	Float life	12	Years
	Initial/replacement costs	300/280	\$/kWh
	O&M cost	4	\$/kWh/year
	Round-trip efficiency	85	%
	Minimum SOC	30	%
Converter	Lifetime	25	Years
	Initial/replacement costs	1010/1000	\$/kW
	O&M cost	10	\$/kW/h
	Rated efficiency	90	%
	No-load loss	0.5	%
Water pumping	Tank capacity	400	m^3
	Pump size	20	kW
	Minimum power of the water pump	2.5	kW
	Nominal water flow rate of the pump	60	m^3/h
Hybrid system	Project lifetime	30	Years
	Real interest rate	6	%
	Maximum LOEE	0.01	p.u.

Monthly load data are estimated for the study area with a peak of 149 kW, which is shown in Figure 3. Using typical daily load profiles for each month, the hourly load data are estimated. In addition, Figure 3 depicts the estimated daily water demand for the study area. Available meteorological data for the study area include hourly solar radiation, hourly ambient temperature, and hourly wind speed [27]. The monthly averages of the meteorological data are shown in Figures 4 and 5.

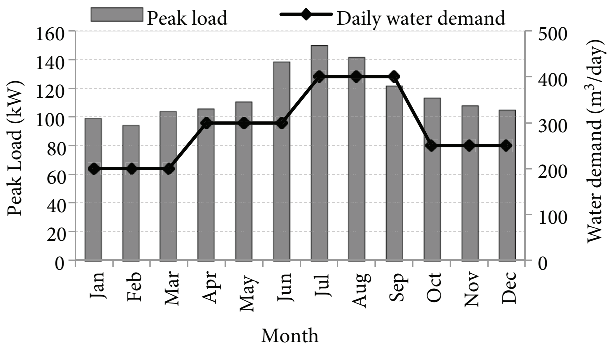

Figure 3. Monthly peak load and daily water demand.

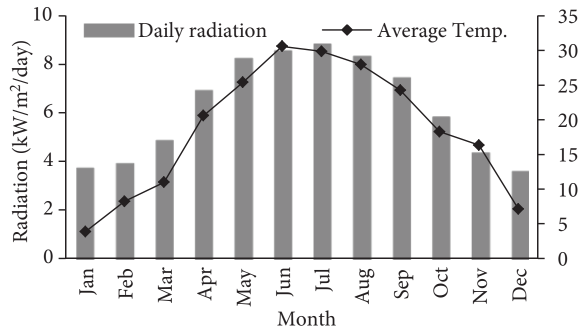

Figure 4. Solar radiation and ambient temperature [27].

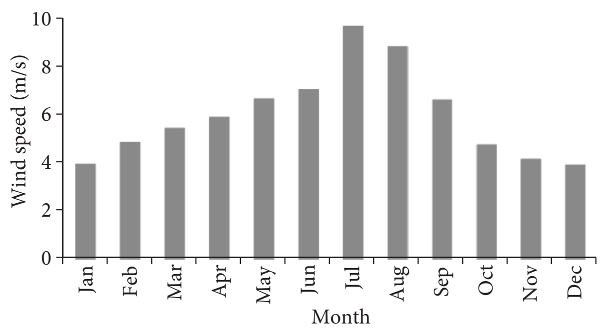

Figure 5. Monthly average wind speed [27].

In Section 4.2, the performance of the proposed optimization algorithm is analyzed neglecting the load growth. The impacts of considering various load growth and wind speed scenarios on the optimization results are investigated in Section 4.3.

4.1. PSOPC parameter selection

The acceleration coefficients and population size of the PSOPC algorithm are selected based on a grid search, which is executed in 2 steps. First, c_3 is set to 0, and for each population size of $P = 20$, 30, 40, and 50, c_1 and c_2 are changed from 1 to 2 in steps of 0.1 (only 1 parameter is changed each time). For each pair of c_1 and c_2, the developed optimization code is run 10 times for Configuration 1, and 2 of the best results are used. Next, for each pair of c_1 and c_2, parameter c_3 is changed from 0 to 1 in steps of 0.1. The best results associated with the steps, with CPSO and PSOPC, are shown in Table 4. Based on Table 4, the PSOPC parameters are selected as $c_1 = 1.4$, $c_2 = 1.4$, $c_3 = 0.8$, and $P = 40$.

Table 4. The best results for various population sizes and PSOPC parameters.

P	c_1	c_2	c_3	NPC ($)	c_1	c_2	c_3	NPC ($)
20	1.3	1.5	0	1,332,633	1.3	1.5	0	1,332,633
	1.8	1.7	0	1,332,802	1.8	1.7	0.5	1,332,430
30	1.6	1.6	0	1,332,392	1.6	1.6	0.8	1,332,165
	1.1	1.7	0	1,332,463	1.1	1.7	0.7	1,332,235
40	1.4	1.4	0	1,332,291	**1.4**	**1.4**	**0.8**	**1,331,932**
	1.7	1.7	0	1,332,451	1.7	1.7	0.6	1,332,033
50	1.8	1.9	0	1,332,350	1.8	1.9	0.8	1,332,069
	1.8	1.7	0	1,332,403	1.8	1.7	1	1,332,143

4.2. Optimization results neglecting the load growth

In this section, the load growth is assumed to be zero. For the sake of simplicity, the proposed operation strategy is run for a 1-year period to obtain the NPC and LOEE values. Ignoring the load growth and aging effects on the performance of the components, the simulation results are extended to the project lifetime.

Table 5 shows the results of optimizing the HES configurations using the proposed PSOPC algorithm. Figure 6 depicts the convergence trend of the proposed PSOPC algorithm for 2 independent runs. To demonstrate the advantages of optimizing the control set points, the optimization results of 4 configurations, obtained from the proposed PSOPC approach, are compared with those of the PSOPC unit-sizing method given in Table 6. The PSOPC unit-sizing method is similar to the proposed PSOPC method but considers predetermined values (instead of optimized ones) for the set points, as shown in the gray area of Table 6. It deserves mentioning that to assure obtaining global optimum solutions, the abovementioned PSOPC approaches are run 20 times and the best-achieved results are used. Considering the fact that PSO-based optimization algorithms randomly select their starting solutions, running these algorithms several times leads to final solutions with different starting solutions, which ensures that the global minimum is achieved.

In addition, the optimization results obtained from the HOMER software [18] (presented in Table 7) are compared with those of the proposed method. In this regard, the same data and parameters are used in both methods, and the load growth is assumed to be zero.

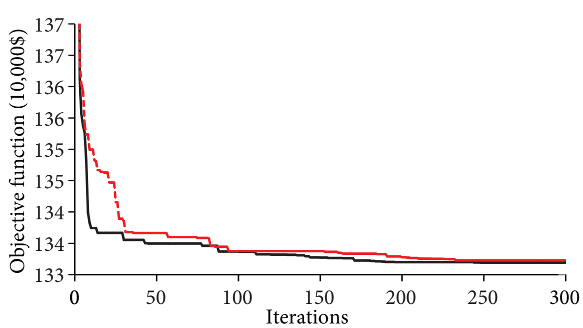

Figure 6. Convergence curves of the proposed PSOPC algorithm (Configuration 1).

Table 5. Optimization results of the HES configurations using the proposed PSOPC.

Configuration	$P_{pv,r}$	$P_{w,r}$	$P_{g,r}$	$P_{c,r}$	$P_{b,r}$	$Slope_{pv}$	$P_{trs,g}$	$P_{lim,b}$	soc_{max}	soc_{sp}	soc_{trs}	NPC	Diesel[1] efficiency	Diesel fuel	Diesel life	Recovered[2] t hermal energy	Excess energy[3] absorbed by deferrable load
	kW	kW	kW	kW	kWh	°	kW	kW	%	%	%	$1000	%	M^3/year	year	MWh/year	%
1	49.8	65.4	43.5	42.9	241.8	33	7.8	39.3	99	96.8	63.4	1331.9	29.5	65.4	3.9	321.8	71.1
2	-	-	82.1	-	-	-	4.5	-	-	-	-	1620.1	25.4	153.5	2.3	740.8	94.5
3	269.7	-	-	108.5	2561	29.6	-	98.3	90.6	-	41.6	2896.6	-	-	-	122.7	20.4
4	67.3	-	47.4	53.1	314.1	26.5	6.2	46.7	97.1	96.3	63.4	1415.1	29.5	90.1	3.1	436.2	85.6

[1] Electrical effciency without considering heat recovery.

[2] Annual thermal energy produced by recovering the waste heat of the diesel generator and dump load.

[3] Fraction of the excess energy of the system that is absorbed by the deferrable load (water pump).

Table 6. Optimization results of the HES configurations using the PSOPC unit-sizing.

Configuration	$P_{pv,r}$	$P_{w,r}$	$P_{g,r}$	$P_{c,r}$	$P_{b,r}$	$Slope_{pv}$	$P_{trs,g}$	$P_{lim,b}$	soc_{max}	soc_{sp}	soc_{trs}	NPC	Diesel[1] efficiency	Diesel fuel	Diesel life	Recovered[2] thermal energy	Excess energy[3] absorbed by deferrable load
	kW	kW	kW	kW	kWh	°	kW	kW	%	%	%	$1000	%	M^3/year	year	MWh/year	%
1	39.7	69.2	41.5	37	245.8	**32.8**	**0**	∞	**100**	**100**	**30**	1341.1	29.2	70.6	3.4	346.7	68.7
2	-	-	82.1	-	-	**-**	**0**	**-**	**-**	**-**	**-**	1620.3	25.4	153.5	2.3	740.9	94.3
3	273.8	-	-	105.2	2542	**32.8**	**-**	∞	**100**	**-**	**30**	2913.2	-	-	-	131.9	19.3
4	60.3	-	49.5	49.8	276.6	**32.8**	**0**	∞	**100**	**100**	**30**	1421.2	29.2	95.6	2.9	461.7	83.6

[1] Electrical effciency without considering heat recovery.

[2] Annual thermal energy produced by recovering the waste heat of the diesel generator and dump load.

[3] Fraction of the excess energy of the system that is absorbed by the deferrable load (water pump).

Table 7. Optimization results of the HES configurations using HOMER software.

Configuration	$P_{pv,r}$	$P_{w,r}$	$P_{g,r}$	$P_{c,r}$	$P_{b,r}$	NPC	Diesel[1] efficiency	Diesel fuel	**Diesel life**	**Recovered[2] thermal energy**
	kW	kW	kW	kW	kWh	$1000	%	M^3/year	**year**	**MWh/year**
1	28.2	68	48.2	32	243.2	1348.2	29.1	78.6	**3.5**	**28.2**
2	-	-	83.4	-	-	1628.2	25.1	157	**2.5**	**-**
3	266.2	-	-	106	2614	2915.1	-	-	**-**	**266.2**
4	55.9	-	50.2	54	334.4	1429.4	29.6	96.5	**3.1**	**55.9**

[1] Electrical efficiency without considering heat recovery.

[2] Annual thermal energy produced by recovering the waste heat of the diesel generator and dump load.

The results presented in Tables 5, 6, and 7 demonstrate that the proposed PSOPC method achieves lower NPC and fuel consumption in all of the configurations in comparison with the other methods. In Configuration 1, the proposed PSOPC selects a larger PV and converter than those associated with the other methods and incurs more initial and replacement costs. However, in the proposed PSOPC method, due to fewer operating hours of the diesel generator as well as its better efficiency, the fuel and O&M costs are less than those of the other methods. Therefore, the NPC in the proposed method, due to its ability in optimizing the control set points, is less than that of the other methods. Consequently, optimizing the control set points of the HES significantly improves the optimization performance.

Latitude-tilted PV panels generate maximum energy during a year [28]. It can be seen from Table 5 that the optimum value of $Slope_{pv}$ for Configuration 1 is 33°, which is close to the latitude of the study area (32.78°). For Configurations 3 and 4, the proposed algorithm determines the PV slope to be smaller than the latitude. In other words, in configurations with no wind turbine, the optimization algorithm decreases $Slope_{pv}$ to ensure more PV production during the summer.

According to Table 5, the optimum value of soc_{sp} is 96.8% in Configuration 1. This indicates that the load following strategy is economical only at high SOC values. The 'excess energy absorbed by deferrable load' column in Table 5 shows that more than 71% of the total surplus energy (in Configuration 1/proposed PSOPC) is absorbed by the deferrable load. In addition, using the recovered thermal energy of the system to supply the thermal loads, the proposed scheme achieves 81% efficiency, which indicates the efficient use of the energy resources. Figure 7 depicts the monthly average daily thermal energy that is recovered from the HES.

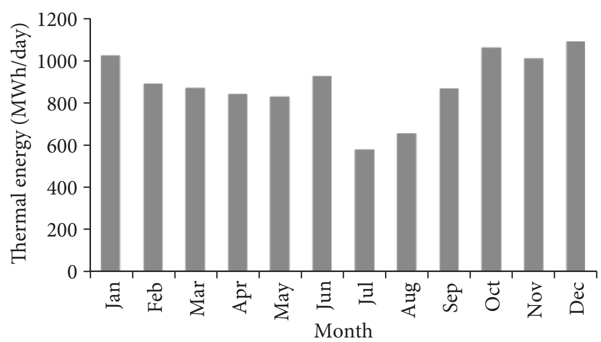

Figure 7. Daily average recovered thermal energy (Configuration 1).

The energy contribution of renewable resources is desired to be as high as possible. Figure 8 shows the annual electrical energy produced by the power sources, which reveals that in Configuration 1, the proposed PSOPC achieves 54% energy contribution of renewable resources compared to 50% in PSOPC unit-sizing and 44% in HOMER. Figure 9 presents the monthly energy produced by the power resources (Configuration 1/proposed PSOPC) and the monthly served energy to the electrical load. Figure 9 shows that the energy produced by the renewable resources reaches its maximum value between March and September (e.g., in July, renewable resources provide 79% of the total generated energy).

The hourly simulation results of Configuration 1 for 13 July are depicted in Figure 10. The charge and discharge powers of the battery are, respectively, illustrated as negative and positive values in Figure 10a. The AC output power of the inverter and AC input power of the rectifier are, respectively, represented by the positive and negative values of the converter power. During night and early morning (when the PV power is zero), the difference between the converter and battery powers represents the losses of the converter. According to Figure 10b, the diesel generator operates when there is a shortage in the renewable powers (hours 1, 3, and 18–23). Using the battery is preferred to the diesel generator during hours 7–9, 15, and 17, when the battery is more economical than the generator. During hours 10–14, renewable resources meet the electrical load, charge the battery, and serve the water pump and dump load. Despite operating the generator at full power and discharging the battery, there is some unmet power at hours 19 and 20 (due to high load, low wind power, and no solar radiation). According to Figure 10b, the water pump absorbs surplus renewable power (approximately 125 kWh) and pumps approximately 375 m^3 of water during the day.

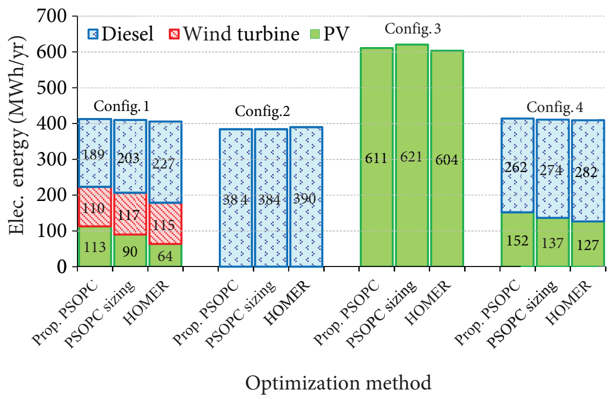

Figure 8. Electrical energy production of power resources.

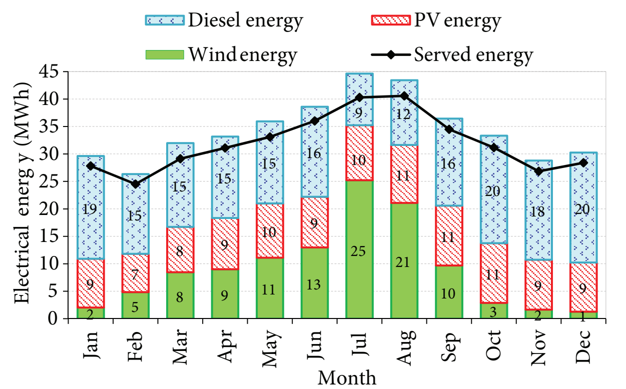

Figure 9. Monthly electrical energy of power resources (Configuration 1).

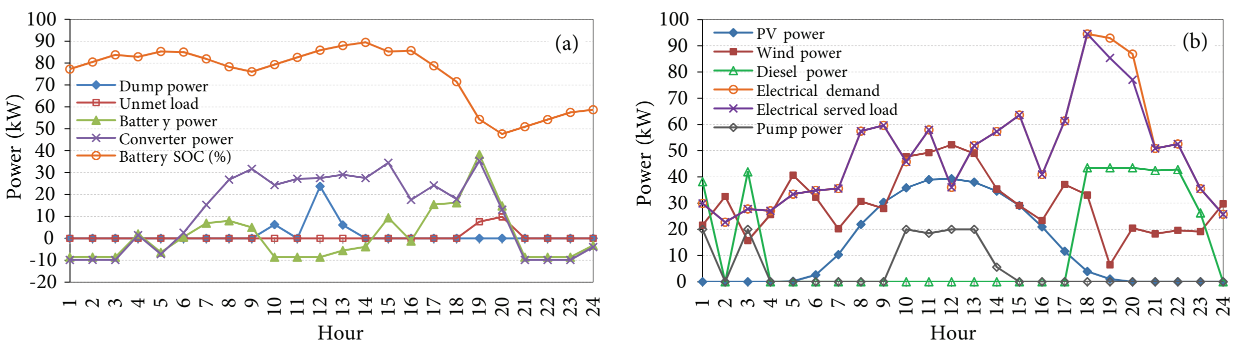

Figure 10. Simulation results of Configuration 1 on 13 July.

Figure 11 shows the water content of the tank (Configuration 1/proposed PSOPC). It is clear that the water content of the tank is kept above the critical water level (25%), except in power shortages during summer.

According to Tables 5, 6, and 7, Configuration 2 has higher NPC, lower diesel efficiency, less diesel lifetime, and more fuel consumption in comparison with Configuration 1. In addition, the results reveal that Configuration 3 is not economical for the study area. The reason for this is that it requires a very large battery bank and incurs very high NPC compared to other configurations.

According to Tables 5, 6, and 7, the proposed PSOPC attains less NPC than the other methods in Configuration 4. Clearly, from Figure 8, the proposed PSOPC achieves a higher energy contribution of the PV than the other methods in Configuration 4.

As a result, Configuration 1 is the best alternative to supply the demands of the study area from the cost, fuel consumption, diesel generator lifetime, and energy contribution of renewable resources points of view.

Furthermore, the proposed PSOPC achieves the best results compared to other methods. Configuration 4 can be selected to supply the study area as the next alternative if a simpler configuration is preferred.

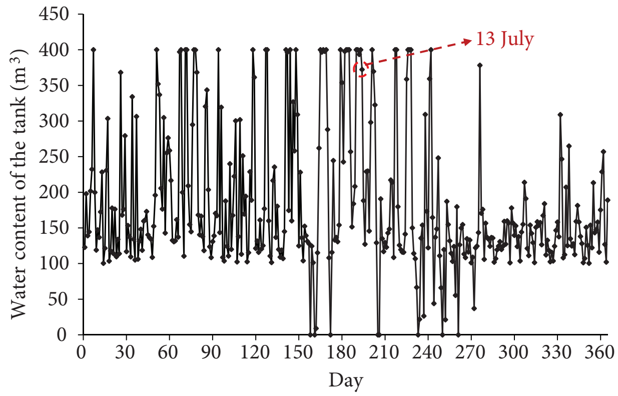

Figure 11. Water content of the tank (Configuration 1).

4.3. Optimization results considering load growth and wind speed scenarios

Possible load growth scenarios for the study area are considered to investigate their impacts on the optimization results. Wind speed is another uncertainty involved in the optimization problem. Wind speed is a random parameter and its variations should be taken into account to achieve a reliable HES design. Investigated are 12 possible scenarios, including 4 annual load growth rates (0, 2%, 5%, and 8%) and 3 wind conditions (baseline wind speed, 10% increase, and 10% decrease). The annual growth rate for the water demand is assumed to be 2%.

It is assumed that the HES should be designed and optimized to supply the growing demands of the study area in the next 5 years with an acceptable level of reliability. The HES can be upgraded after 5 years if necessary. The study results presented in this section focus on the first 5 years, and system upgrading is not studied in this paper. The optimal generation expansion planning of the HES considering the load growth would be our future work.

At each iteration of the PSOPC algorithm and for each particle, the proposed operation strategy is run for the first year of the planning horizon, as described in Section 2.8. The proposed operation strategy is run for the next years, while the values obtained for the battery SOC, as well as the water tank level at the end of each year, are considered as the initial values for the next year.

The NPC can be calculated using Eq. (9), considering $N_{pr} = 5$. In Eq. (9), the term $C_I + C_{rep}^{PW} - S^{PW}$ indicates the usage cost (the cost related to decreasing the useful lifetime of the components) in the first 5 years of the project lifetime.

Figures 12–15 present the best results of optimizing the abovementioned scenarios after 20 trials of the proposed PSOPC algorithm for Configuration 1. Figures 12 and 13 show the optimal values of the component size and control set points for 12 scenarios, respectively. These 2 figures help the decision maker to consider the impacts of the load growth and wind speed uncertainties in the decision-making process. It can be seen from Figure 12 that the component size increase as the load growth increases. The size of the wind turbine is highly sensitive to wind speed variations. However, the size of the diesel generator is not sensitive to wind speed variations. Clearly, with a 10% increase in the wind speed, the optimization algorithm prefers the wind turbine to the PV array. Figure 13 depicts the optimal values of the control set points for 12 scenarios. It can be seen from Figure 13 that $SOC_{\max}$ and SOC_{sp} remain approximately constant in all of the scenarios.

The slope of the PV panel, $slope_{pv}$, increases in scenarios with low wind speed to produce more energy during summer and to compensate for the wind energy reduction. Figure 14 illustrates the costs associated with the 5-year operation of the HES, where it can be clearly seen that the cost associated with scenarios with high wind speed and low load growth is lower compared to that of other scenarios. Additionally, with a 10% decrease in the wind speed, the diesel generator operates for more hours and consumes more fuel, resulting in higher O&M and fuel costs. Figure 14 can be used to compare the relative importance of each cost type. In this regard, the NPC of the HES is considerably affected by the usage cost and fuel cost, and the O&M cost has less impact compared to the other cost types.

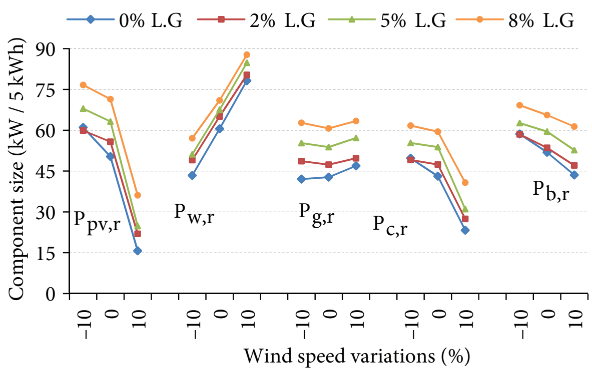

Figure 12. Optimal component size for 12 scenarios ($P_{b,r}$ is divided by 5), L.G: load growth.

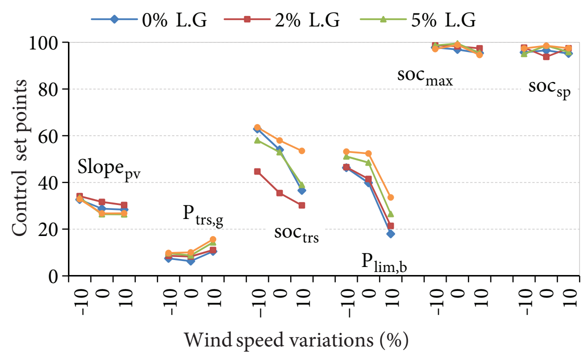

Figure 13. Optimal control set points for 12 scenarios, L.G: load growth.

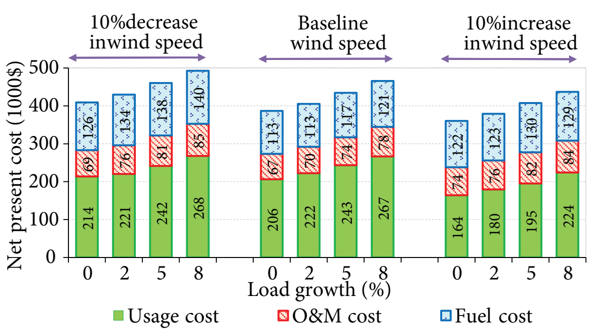

Figure 14. Contribution of several cost types in the NPC.

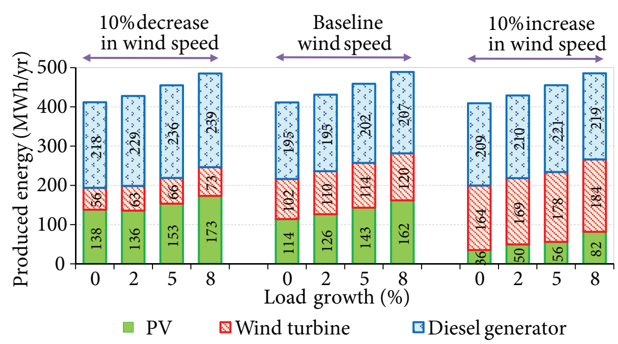

Figure 15. Average energy production over 5 years.

Figure 15 depicts the energy contribution of the diesel generator and renewable resources. It can be seen that scenarios with a higher load growth achieve a better contribution of renewable resources. As expected in scenarios with a higher wind speed, the energy produced by the wind turbine rapidly increases, while the energy produced by the PV array decreases.

5. Conclusion

This paper presents a new method to optimize standalone HESs using the PSOPC approach. The proposed optimization procedure considers 2 aspects of the unit-sizing and operation strategy, which are both correlated and should be optimized simultaneously. The proposed method minimizes the NPC objective function, while it maintains the physical and reliability constraints. New set points for the control system are proposed, and a new operation strategy based on the proposed set points is developed. The code, developed in MATLAB, can optimize various HES configurations and integrate other components as needed. Numerical studies were conducted, using the load profile and meteorological data of an area in the eastern part of Iran, to demonstrate the effectiveness of the proposed method. Four HES configurations were investigated using the proposed optimization algorithm and HOMER software package. The results presented demonstrate the superiority of the proposed approach and confirm that the wind/PV/diesel/battery system is the most cost-effective and reliable HES for the study area. Comparing the proposed approach with a similar method, for which its control set points are set to predetermined values (instead of optimized ones), verifies the effectiveness of the proposed set points.

In addition, possible load growth scenarios for the near future, as well as various wind conditions, were investigated. The results obtained from the scenario analyses show that the optimal component size of the HES, as well as its optimal operation, are sensitive to the load growth and wind speed variations. From the results presented, it can be concluded that factors such as load growth and wind speed uncertainties should also be considered in optimizing the HES to achieve a reliable and cost-effective hybrid system.

Nomenclature

A_{pv}	Area of the PV array (m^2)
c_1, c_2, c_3	Acceleration constants of PSOPC algorithm
c_f	Fuel price (\$/L)
C_{tank}	Capacity of the water tank (m^3)
D_w^d	Daily water demand (m^3/day)
E_d^t	Electrical energy demand (kWh)
ENS^t	Energy not served (kWh)
F_0	No-load fuel consumption of the diesel generator (L/h/kW$_{rated}$)
F_1	Incremental fuel consumption of the diesel generator (L/kWh$_{out}$)
F_g^N	Fuel consumption of the diesel generator during year N (L/year)
$F_{P,\max}$	Nominal water flow rate of the pump (m^3/h)
$Gbest^k$	The best position found by the swarm up to iteration k
G_T^t	Incident radiation on tilted PV panels (kW/m^2)
i	Real interest rate
$LOEE_{p.u.}^{ann}$	Annual LOEE (p.u.)
$LOEE_{p.u.}^{\max}$	Maximum allowable LOEE (p.u.)
m	Component type (PV, wind turbine, diesel generator, battery, converter)
N_{pr}	Project lifetime (years)
$Pbest_i^k$	The best previously visited position of particle i up to iteration k
$P_{b,r}$	Rated capacity of the battery bank (kWh)
$P_{c,in}^t$	Converter input power (kW)
$P_{c,NL}$	No-load loss of the converter (kW)
$P_{c,r}$	Converter rated power (kW)
P_{dump}^t	Input power to the dump load (kW)
$P_{g,min}$	Minimum loading of diesel generator (kW)
$P_{g,r}$	Rated power of the diesel generator (kW)
P_L^t	Electrical load (kW)
$P_{lim,b}$	Battery discharge power limit (kW)
$P_{m,r}$	Rated power/capacity of component m (kW/kWh)
P_p^t	Input power to the water pump (kW)
$P_{p,r}$	Rated power of the water pump (kW)
$P_{p,\min}$	Minimum power of the water pump (kW)
$P_{pv,r}$	Rated power of the PV array (kW)
$P_{trs,g}$	Running threshold of the diesel generator (kW)
$P_{w,r}$	Rated power of the wind turbine (kW)
P_w^t	Output power of the wind turbine (kW)
r_1^k, r_2^k, r_3^k	Uniform random number generators in a range of (0 , 1)
$Rbest_d^k$	Passive congregator at iteration k
R_g^N	Annual operating hours of diesel generator (h/year)
$Slope_{pv}$	Slope of the PV panels (degrees)
$soc_{\max}$	Maximum SOC of the battery (%)
soc_{sp}	SOC set point of battery (%)
soc_{trs}	SOC threshold of battery (%)
U_g^t	Diesel generator dispatch indicator (0 means OFF, 1 means ON)
V_i^k	Velocity vector of particle i at iteration k
W_{tank}^d	Water content of the tank at the end of day d (m^3)
X_i^k	Position vector of particle i at iteration k
$\alpha_{m,I}$, $\alpha_{m,rep}$	Initial and replacement costs per kW/kWh of component m
$\alpha_{m,om}$	O&M cost per kW/kWh of component m
$\eta_{c,r}$	Converter efficiency at rated power

η_{mp}^{t}	Maximum power point efficiency of the PV array
η_{mppt}	Efficiency of the maximum power point tracker
$\eta_{mp,STC}$	Maximum power point efficiency of the PV array under standard test conditions
ω^{k}	Inertia factor of the PSOPC algorithm
χ	Constriction factor associated with the particle's velocity

References

[1] W. Zhou, C. Lou, Z. Li, L. Lu, H. Yang, "Current status of research on optimum sizing of stand-alone hybrid solar-wind power generation systems", Applied Energy, Vol. 87, pp. 380–389, 2010.

[2] B. Dursun, C. Gökçöl, "Economic analysis of a wind-battery hybrid system: an application for a house in Gebze, Turkey, with moderate wind energy potential", Turkish Journal of Electrical Engineering and Computer Sciences, Vol. 20, pp. 319–333, 2012.

[3] M. Mohammadi, S.H. Hosseinian, G.B. Gharehpetian, "GA-based optimal sizing of microgrid and DG units under pool and hybrid electricity markets", International Journal of Electrical Power and Energy Systems, Vol. 35, pp. 83–92, 2012.

[4] L. Wang, C. Singh, "Multicriteria design of hybrid power generation systems based on a modified particle swarm optimization algorithm", IEEE Transactions on Energy Conversion, Vol. 24, pp. 163–172, 2009.

[5] A. Kashefi Kaviani, G.H. Riahy, S.H.M. Kouhsari, "Optimal design of a reliable hydrogen-based stand-alone wind/PV generating system, considering component outages", Renewable Energy, Vol. 34, pp. 2380–2390, 2009.

[6] U. Boonbumroong, N. Pratinthong, S. Thepa, C. Jivacate, W. Pridasawas, "Particle swarm optimization for AC-coupling standalone hybrid power systems", Solar Energy, Vol. 85, pp. 560–569, 2011.

[7] S.M. Hakimi, S.M. Moghaddas-Tafreshi, "Optimal sizing of a stand-alone hybrid power system via particle swarm optimization for Kahnouj area in south-east of Iran", Renewable Energy, Vol. 34, pp. 1855–1862, 2009.

[8] C.D. Barley, C.B. Winn, "Optimal dispatch strategy in remote hybrid power systems", Solar Energy, Vol. 58, pp. 165–179, 1996.

[9] M. Ashari, C.V. Nayar, "An Optimum dispatch strategy using set points for a photovoltaic-diesel battery hybrid power system", Solar Energy, Vol. 66, pp. 1–9, 1999.

[10] A. Gupta, R.P. Saini, M.P. Sharma, "Modelling of hybrid energy system–Part II: Combined dispatch strategies and solution algorithm", Renewable Energy, Vol. 36, pp. 466–473, 2011.

[11] S.A. Pourmousavi, M.H. Nehrir, C.M. Colson, C. Wang, "Real-time energy management of a stand-alone hybrid wind-microturbine energy system using particle swarm optimization", IEEE Transactions on Sustainable Energy, Vol. 1, pp. 193–201, 2010.

[12] R. Dufo-López, J.L. Bernal-Agustín, J. Contreras, "Optimization of control strategies for stand-alone renewable energy systems with hydrogen storage", Renewable Energy, Vol. 32, pp. 1102–1126, 2007.

[13] R. Dufo-López, J.L. Bernal-Agustín, J.M. Yusta-Loyo, J.A. Domínguez-Navarro, I.J. Ramírez-Rosado, J. Lujano, I Aso, "Multi-objective optimization minimizing cost and life cycle emissions of stand-alone PV-wind-diesel systems with batteries storage", Applied Energy, Vol. 88, pp. 4033–4041, 2011.

[14] Z.W. Geem, "Size optimization for a hybrid photovoltaic–wind energy system", International Journal of Electrical Power and Energy Systems, Vol. 42, pp. 448–451, 2012.

[15] J.A. Duffie, W.A. Beckman, Solar Engineering of Thermal Processes, New York, NY, USA, Wiley, 2006.

[16] S. Zekai, Solar Energy Fundamentals and Modeling Techniques: Atmosphere, Environment, Climate Change and Renewable Energy, New York, NY, USA, Springer, 2008.

[17] Seaforth Energy, Atlantic Orient AOC 15/50 Specifications, Dartmouth, Nova Scotia, Canada, 2012, available at http://seaforthenergy.com/aoc-1550/.

[18] HOMER, The Hybrid Optimization Model for Electric Renewables, HOMER Energy LLC, Boulder, CO, USA, 2012, available at http://www.homerenergy.com.

[19] O. Skarstein, K. Ulhen, "Design considerations with respect to long-term diesel saving in wind/diesel plants", Wind Engineering, Vol. 13, pp. 72–87, 1989.

[20] J.F. Manwell, J.G. McGowan, "A lead acid battery storage model for hybrid energy systems", Solar Energy, Vol. 50, pp. 399–405, 1993.

[21] J.F. Manwell, A. Rogers, G. Hayman, C.A. Avelar, J.G. McGowan, U. Abdulwahid, K. Wu, "Hybrid2-a hybrid system simulation model: theory manual", 2012, available at http://www.ceere.org/rerl/projects/software/hybrid2.

[22] H. Wenzl, I. Baring-Gould, R. Kaiser, B.Y. Liaw, P. Lundsager, J. Manwell, A. Ruddell, "Life prediction of batteries for selecting the technically most suitable and cost effective battery", Journal of Power Sources, Vol. 144, pp. 373–384, 2005.

[23] G.M. Masters, Renewable and Efficient Electric Power Systems, New York, NY, USA, Wiley, 2004.

[24] Y. Del Valle, G.K. Venayagamoorthy, S. Mohagheghi, J.C. Hernandez, R.G. Harley, "Particle swarm optimization: basic concepts, variants and applications in power systems", IEEE Transactions on Evolutionary Computation, Vol. 12, pp. 171–195, 2008.

[25] S. He, Q.H. Wu, J.Y. Wen, J.R. Saunders, R.C. Paton, "A particle swarm optimizer with passive congregation", Biosystems, Vol. 78, pp. 135–147, 2004.

[26] J.G. Vlachogiannis, K.Y. Lee, "A comparative study on particle swarm optimization for optimal steady state performance of power systems", IEEE Transactions on Power Systems, Vol. 21, pp. 1718–1728, 2006.

[27] Renewable Energy Organization of Iran (SUNA), Meteorological Data, Tehran, Iran, 2012, available at http://www.suna.org.ir/en/home.

[28] Y.P. Chang, "Optimal tilt angles for photovoltaic modules in Taiwan", International Journal of Electrical Power and Energy Systems, Vol. 32, pp. 956–964, 2010.